



REPORT

 OPEN ACCESS

Broad epitope coverage of a human *in vitro* antibody library

Arvind Sivasubramanian^a, Patricia Estep ^a, Heather Lynaugh^a, Yao Yu^{a,**}, Adam Miles^b, Josh Eckman^b, Kevin Schutz^a, Crystal Piffath^a, Nadthakarn Boland^a, Rebecca Hurley Niles ^a, Stéphanie Durand^a, Todd Boland^a, Maximiliano Vásquez^a, Yingda Xu^a, and Yasmina Abdiche^{c,*}

^aAdimab LLC, Lebanon, NH, USA; ^bWasatch Microfluidics, Inc., Salt Lake City, UT, USA; ^cRinat-Pfizer, Inc., South San Francisco, CA, USA

ABSTRACT

Successful discovery of therapeutic antibodies hinges on the identification of appropriate affinity binders targeting a diversity of molecular epitopes presented by the antigen. Antibody campaigns that yield such broad “epitope coverage” increase the likelihood of identifying candidates with the desired biological functions. Accordingly, epitope binning assays are employed in the early discovery stages to partition antibodies into epitope families or “bins” and prioritize leads for further characterization and optimization. The collaborative program described here, which used hen egg white lysozyme (HEL) as a model antigen, combined 3 key capabilities: 1) access to a diverse panel of antibodies selected from a human *in vitro* antibody library; 2) application of state-of-the-art high-throughput epitope binning; and 3) analysis and interpretation of the epitope binning data with reference to an exhaustive set of published antibody:HEL co-crystal structures. Binning experiments on a large merged panel of antibodies containing clones from the library and the literature revealed that the inferred epitopes for the library clones overlapped with, and extended beyond, the known structural epitopes. Our analysis revealed that nearly the entire solvent-exposed surface of HEL is antigenic, as has been proposed for protein antigens in general. The data further demonstrated that synthetic antibody repertoires provide as wide epitope coverage as those obtained from animal immunizations. The work highlights molecular insights contributed by increasingly higher-throughput binning methods and their broad utility to guide the discovery of therapeutic antibodies representing a diverse set of functional epitopes.

ARTICLE HISTORY

Received 29 August 2016
Revised 30 September 2016
Accepted 3 October 2016

KEYWORDS

Biosensor; epitope; epitope binning; epitope coverage; hen egg white lysozyme; therapeutic monoclonal antibody

Introduction

The biopharmaceutical industry invests heavily in the discovery and clinical development of monoclonal antibodies (herein referred to as “antibodies”), which generates demand for higher throughput analytical tools that can meet this capacity.¹ An antibody’s epitope specificity largely dictates its biological function, and, since it is an innate property that cannot be optimized rationally by engineering, it must be selected properly. In early-stage therapeutic antibody discovery, the aim is often to identify clones that target a broad range of epitopes on the specific antigen of interest and prioritize those with the desired biological function. The vast genetic diversity of state-of-the-art antibody libraries and optimized selection methods enable the discovery of functionally effective and mechanistically differentiated binders.^{2,3} Sourcing antibodies from both *in vivo* and *in vitro* platforms may maximize epitope diversity opportunities, given their complementary strengths and limitations.^{4–6}

High-throughput antibody generation methods must be used with advanced analytical methods to efficiently characterize their outputs and enable a more informed selection of antibodies with therapeutically relevant epitopes. High-throughput


epitope binning methods on label-free biosensors are particularly useful in this regard because the results from these experiments allow antibodies to be sorted into epitope “families” or “bins” based upon their ability to cross-block one another’s binding to their antigen in a combinatorial and pairwise fashion.⁷ These methods can also discern fine specificities that can be used to discriminate antibodies with near-identical epitopes, which may manifest as functional differences, or offer intellectual property opportunities.

Here, we describe a collaborative effort in which we applied state-of-the-art label-free analytical methods developed at Rinat-Pfizer to characterize the epitope coverage of antibodies derived from Adimab’s yeast-based library and compare it with the collective epitope coverage of antibodies drawn from the literature against the same target. As a model antigen, we chose hen egg white lysozyme (HEL) because of the wealth of epitope information available on this target in the form of published co-crystal structures representing 20 unique antibodies derived primarily from *in vivo* sources (the “structural benchmark”), binding to different HEL epitopes. We also illustrate how high-throughput binning methods can be used to reveal the intricate epitope

CONTACT Arvind Sivasubramanian  arvind.sivasubramanian@adimab.com; Yasmina Abdiche  Yabdiche@microfl.com, ynoubia@gmail.com

*Present address: Wasatch Microfluidics, Inc, Salt Lake City, UT, USA.

**Present address: Merck and Co, Palo Alto, CA, USA.

 Supplemental data for this article can be accessed on the [publisher’s website](#).

Published with license by Taylor & Francis Group, LLC © Arvind Sivasubramanian, Patricia Estep, Heather Lynaugh, Yao Yu, Adam Miles, Josh Eckman, Kevin Schutz, Crystal Piffath, Nadthakarn Boland, Rebecca Hurley Niles, Stéphanie Durand, Todd Boland, Maximiliano Vásquez, Yingda Xu, and Yasmina Abdiche

This is an Open Access article distributed under the terms of the Creative Commons Attribution-Non-Commercial License (<http://creativecommons.org/licenses/by-nc/3.0/>), which permits unrestricted non-commercial use, distribution, and reproduction in any medium, provided the original work is properly cited. The moral rights of the named author(s) have been asserted.

diversity of antibody libraries, thereby informing early-stage discovery of therapeutic antibodies when it is advantageous to identify antibodies representing a diversity of functional epitopes for lead development.

Results

The results are presented in the following order. First, we outline the steps involved in library selections, kinetic characterization of HEL binders, epitope binning and selection of the literature controls. We then present the experimental cross-blocking data for 7 control antibodies considered as an isolated subset and retrospectively validate a structure-based metric that correctly predicts these results. Next, we deploy this metric to predict a cross-blocking matrix of the set of 20 literature controls to gain insight into the epitope coverage of the entire structural benchmark. Finally, we present the experimental binning data for the entire set of library clones and 7 controls, and compare the epitope coverage of the library to that of the structural benchmark.

Binning study of 350 anti-HEL antibodies discovered via selections using a human *in vitro* library

Selections were performed against monomeric HEL antigen using the Adimab synthetic IgG antibody library (see Methods).^{8,9} A panel of 350 antibodies was included in the binning study based on their confirmed binding in an Octet screening assay¹⁰ toward soluble HEL and sequence uniqueness. The antibody variable region sequences mapped to light chain germline families V κ 1, V κ 2, V κ 3 and V κ 4 and heavy chain germline families VH1, VH3, VH4, and VH5. Thirteen of the 16 possible VH:V κ germline family pairings are represented in this antibody panel. Five pairs, VH3:V κ 1, VH4:V κ 3, VH4:V κ 1, VH3:V κ 3 and VH1:V κ 1, accounted for 77% of the panel (Table S1). The complementarity-determining region (CDR) H3 length (IMGT definition)¹¹ ranged from 10 to 23 amino acids (AA) with a median of 15 AA (the library design comprised lengths 4 to 31 AA); L3 lengths ranged from 8–10 AA with 9-AA L3 sequences comprising the majority (85%) in line with the input library design. The polyreactivity of the antibody clones was

assessed using a previously published protocol^{9,12} and categorized into low (72%), medium (8%) and high (20%) levels based on poly-specificity reagent mean fluorescence intensity (PSR MFI) cutoffs of 200, 500 and > 500, respectively. While low polyreactivity is generally desired, clones that exhibited medium to high PSR binding levels were retained because this property can be optimized by engineering,⁹ if clones have interesting enough epitopes to warrant their further development.

The panel of library anti-HEL antibodies exhibited diverse binding kinetics, informing the design of the epitope binning experiments

To assess the affinity range of the antibodies used in this study, we used a ProteOn XPR36 surface plasmon resonance (SPR) biosensor and characterized the binding kinetics of HEL toward a panel of 7 control antibodies, CTL-1, 2, 3, 4/4*, and 5/5*, chosen from the literature (discussed subsequently) and the panel of library clones. The apparent equilibrium dissociation constants (K_D values) for the controls ranged from ~20 pM to 1 nM, mostly showing very slow dissociation rate constants (k_d values of $\sim 2 \times 10^{-4} \text{ s}^{-1}$), approaching the resolution of the employed capture-based approach (Table 1). In contrast, the library was kinetically diverse, showing apparent K_D values ranging from 82 pM to 69 nM, with the majority of clones in the single digit nM range, and having relatively fast k_d values (4×10^{-3} to 0.13 s^{-1}). Representative examples of the global kinetic analysis are shown in Fig. 1A, and an isoaffinity plot of the kinetic rate constants obtained for the entire study is provided in Fig. 1B.

Characterizing the binding kinetics of the antibodies guided the design of our array-based SPR imaging epitope binning assays because clones with fast k_d values are generally ill-suited as capture antibodies (or “ligands”) when coupled to the chip. To mitigate this limitation, we employed a “co-injection” approach to sample delivery in our binning experiments whereby an injection of HEL was followed immediately by an injection of solution antibody (analyte), thereby minimizing the time allowed for HEL to dissociate from the ligand array during the sandwiching step. The single flow cell configuration employed by array-based SPR imaging relied on the use of a universal regeneration condition that did not work perfectly for all ligands. To compensate for ligand attrition in

Table 1. SPR affinity determinations of HEL/anti-HEL antibody binding interactions. A one-shot kinetic method was used on a ProteOn XPR36 biosensor to determine the affinity of solution HEL binding to immobilized antibodies; all antibodies were reformatted into human IgG1 and captured via goat anti-human-IgG (Fc-specific) reagent coated on NLC or GLC chips. The values reported for the literature controls are the mean (and standard deviation) of N replicates. See Fig. 1.

Antibody		k_a (1/Ms)	k_d (1/s)	K_D (nM)
Literature controls				
D1.3	CTL-1	$2.9 (1.3) \times 10^6$	$3.2 (0.4) \times 10^{-3}$	1.21 (0.36) $n = 5$
D11.15	CTL-2	$4.4 (1.6) \times 10^6$	$5.5 (1.3) \times 10^{-3}$	1.35 (0.42) $n = 5$
cAb-Lys3	CTL-3	$2.2 (0.9) \times 10^6$	$1.1 (0.5) \times 10^{-3}$	0.52 (0.10) $n = 4$
HyHEL-8	CTL-4	$2.6 (0.7) \times 10^6$	$2.1 (0.7) \times 10^{-4}$	0.083 (0.029) $n = 5$
HyHEL-10	CTL-4*	$2.6 (0.1) \times 10^6$	$1.7 (0.5) \times 10^{-4}$	0.065 (0.019) $n = 4$
F10.6.6	CTL-5	$1.1 (0.3) \times 10^7$	$2.5 (1.5) \times 10^{-4}$	0.024 (0.014) $n = 4$
HyHEL-5	CTL-5*	$9.5 (1.6) \times 10^6$	$2.3 (0.6) \times 10^{-4}$	0.025 (0.010) $n = 5$
<i>In vitro</i> library ($N = 350$ antibodies)				
0% quartile		7.7×10^4	8.2×10^{-5}	0.082
25% quartile		6.1×10^5	3.8×10^{-3}	3.1
50% quartile		1.2×10^6	9.4×10^{-3}	6.8
75% quartile		2.4×10^6	1.7×10^{-2}	15.8
100% quartile		3.0×10^7	1.3×10^{-1}	69

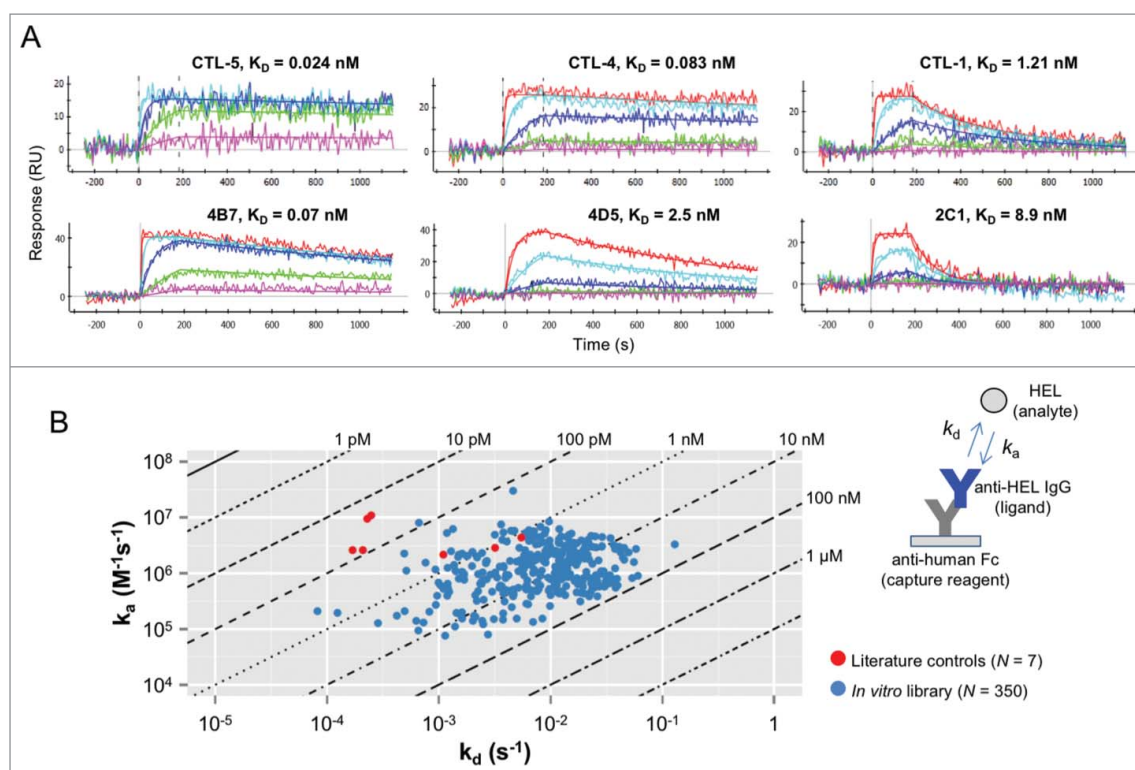


Figure 1. One-shot kinetic analysis of HEL/anti-HEL antibody binding interactions using the ProteOn XPR36 biosensor. (A) Global fits for select clones chosen from the literature (top panel) and the *in vitro* library (bottom panel), where the overlay plots show the measured data (noisy lines) and simulated fit (smooth, color-matched lines). (B) Isoaffinity plot graphing the kinetic rate constants for the entire set of clones used in this study. The inset shows the capture-based assay format employed.

a given epitope binning campaign, we therefore address the entire 2-dimensional “analyte x ligand” interaction matrix. To bypass the need for any regeneration, we also performed lower-throughput epitope binning assays on a subset of clones using the Octet, a commonly used biolayer interferometry (BLI)-based biosensor technology that employs single-use disposable sensors. The complementary strengths and limitations of SPR imaging and Octet technologies in the context of label-free epitope binning assays have been discussed elsewhere.⁷ Further details of the kinetic characterization and epitope binning experiments are provided in the Methods section.

The collective epitope of the 7 controls covers 60% of HEL’s accessible surface area

To benchmark the epitope diversity of the library clones, we sought a panel of control antibodies from the literature with crystallographically-defined epitopes that collectively covered a large area of the HEL surface. Based on a comprehensive search of the Protein Data Bank (PDB),¹³ we identified 79 antibody:lysozyme complexes, 20 of which represent unique antibody sequences. Details of these 20 complexes, constituting the “structural benchmark,” are presented in Table 2. The formatted coordinate files for the complexes are provided as supplementary material. The majority of these antibodies originate from rodent and camelid immunizations ($n = 16$) and a small number ($n = 4$) from *in vitro* library designs. Based on solvent-accessible surface area calculations (data not shown) using the crystal structures, the binding epitopes of the 20 antibodies collectively cover 87% of the lysozyme solvent-accessible surface area of $\sim 6100 \text{ \AA}^2$. To capture

the breadth of epitope coverage found in the literature, we selected a subset of 5 antibodies as primary experimental controls, namely D1.3, D11.15, cAbLys3, HyHEL-8, and F10.6.6, referred to here as CTL-1 through CTL-5, respectively. To probe fine specificities, we added to the control panel HyHEL-10 (CTL-4*) and HyHEL-5 (CTL-5*), which bind near-identical epitopes as their respective counterparts, CTL-4 and CTL-5. Antibodies CTL-1, 4 and 5 have been used in previous HEL epitope binning studies.¹⁴ The camelid antibody (CTL-3) displays an interesting binding mode to the HEL active site using a long CDR3 loop.^{15,16} The 7 controls, whose collective epitope covers 60% of the HEL solvent-accessible surface area, were prepared recombinantly for use in the binning experiments. An additional 12 antibodies in the set (not including Ab_4n1e) increase the coverage to 78%, implying rather low marginal increase per added control. The remaining 9% of the collective epitope is recognized by the VL:VL homodimer (antibody Ab_4n1e) corresponding to PDB entry 4n1e. While this antibody would have been a valuable addition to our control panel, it was deposited into the database after we had finalized the set of controls.

The control antibody panel was critical here to compare and contrast the epitope coverage of the library clones vis-à-vis the structural benchmark. Each antibody was assigned a “blocking profile” (see Methods), which is a single annotation that merges the pairwise cross-blocking data against the control antibodies. The panel of 5 primary controls leads to 32 (2^5) such theoretical profiles, of which 25 were structurally compatible with the simultaneous cross-blocking of at least 2 controls. Since it intersects information related to cross-blocking of control antibodies binding to distinct HEL epitopes, the profile definition is generally

Table 2. Literature anti-HEL antibodies used in *theoretical* structure-based cross-blocking predictions. Unless stated otherwise, the PDB code refers to the co-crystal complex with HEL; complex with ¹pheasant egg lysozyme, ²turkey egg-white lysozyme, ³guinea fowl lysozyme and ⁴human lysozyme. Seven antibodies were selected as controls and prepared recombinantly for use in epitope binning experiments. See Methods and Table 3 for explanation of the blocking profile assignments. The type of the antibody format, i.e., whether standard VL:VH heterodimer (VL:VH), camelid heavy chain only antibody (VHH), heavy chain only antibody (VH) or light chain dimer (VL:VL) is indicated in addition to the source technology. The coordinates corresponding to the light (LC), heavy (HC) and lysozyme (Ag) chain IDs were extracted from each PDB entry and used to compute metrics described in the text.

PDB code	Resolution (Å)	Antibody	Control name	Blocking profile	Construct	Source	PDB chain ID		
							LC	HC	Ag
1vfb	1.80	D1.3	CTL-1	12	VL:VH	Rodent immunization	A	B	C
1jhl ¹	2.40	D11.15	CTL-2	123	VL:VH	Rodent immunization	L	H	A
1jto	2.50	cAbLys3	CTL-3	23	VHH	Camelid immunization	—	A	L
1ndg	1.90	HyHEL-8	CTL-4	4	VL:VH	Rodent immunization	A	B	C
1c08	2.30	HyHEL-10	CTL-4*	4	VL:VH	Rodent immunization	A	B	C
1p2c	2.00	F10.6.6	CTL-5	5	VL:VH	Rodent immunization	A	B	C
1yqv	1.70	HyHEL-5	CTL-5*	5	VL:VH	Rodent immunization	L	H	Y
1dzb ²	2.00	1f9	—	1234	VL:VH	Rodent immunization	A	A	X
1fbi ³	3.00	F9.13.7	—	4	VL:VH	Rodent immunization	L	H	X
1op9 ⁴	1.86	HL6	—	4	VHH	Camelid immunization	—	A	B
1ri8	1.85	1D2L19	—	35	VHH	Camelid immunization	—	A	B
1rjc	1.40	cAb-Lys2	—	235*	VHH	Camelid immunization	—	A	B
1zv5	2.00	D2-L29	—	35	VHH	Camelid immunization	—	A	L
1zvh	1.50	D2-L24	—	5	VHH	Camelid immunization	—	A	L
1zvy	1.63	D3-L11	—	234	VHH	Camelid immunization	—	A	B
4i0c ⁴	1.95	cAbHuL5	—	12	VHH	Camelid immunization	—	D	A
4n1c	1.70	Ab_4n1c	—	123	VL:VL	<i>In vitro</i> library	A/B	—	C
4n1e	2.23	Ab_4n1e	—	0	VL:VL	<i>In vitro</i> library	A/B	—	I
4tsa	2.27	Ab_4tsa	—	123	VL:VH	<i>In vitro</i> library	L	H	A
4u3x	2.26	H04	—	235	VH	<i>In vitro</i> library	—	A	B

indicative of the binding footprint of an antibody. We reasoned that a larger number of observed profiles corresponds to a diversity of binding footprints, and thus broader epitope coverage.

Epitope binning studies confirmed that the 7 literature control antibodies fall into 5 bins when considered as an isolated subset

To establish confidence in the 3D structure-based interpretation of the binning data from the subsequent high-throughput experiments, we first binned the 7 control antibodies against one another using the Octet and validated the results against expectations based on the co-crystal structures. Fig. 2A shows an image of 5 control antibodies, CTL-1 through CTL-5, as ribbon diagrams superposed as an overlay plot on the HEL surface, shown as a white space-filled model. Collectively, it appears that the controls densely cover one face of the HEL surface and occupy 3 non-overlapping regions; (1) CTL-1, 2, and 3; (2) CTL-4; and (3) CTL-5. CTL-1 (blue) and CTL-2 (green) would be predicted to block one another because their epitopes appear to overlap significantly, but it is unclear whether the minimally overlapping epitope contacts between CTL-2 and CTL-3 (red) would be sufficient to manifest as a blocking pair (see Fig. 2A - inset). We employed a classical sandwich assay format, in which a solution antibody (analyte) is tested for binding to HEL that is first captured by an immobilized antibody (ligand). An example of the data obtained on amine-coupled coupled antibody D11.15 (CTL-2) is shown in Fig. 2B. Antibody analytes that showed significant binding responses were classified as “not blocked” (also known as “sandwich pairing” with the coupled antibody), whereas those that showed negligible binding, similar to that of a buffer analyte were classified as “blocked.” By addressing all pairwise permutations of the 7 control mAbs, we generated a comprehensive interaction

matrix, as shown in the heat map of Fig. 2C, where the red and green cells indicate blocking and non-blocking (or sandwiching) pairs, respectively. Five epitope bins emerge from this analysis, populated by (1) CTL-1, (2) CTL-2, (3) CTL-3, (4) CTL-4 and CTL-4*, and (5) CTL-5 and CTL-5*, as graphed in the network blocking plot of Fig. 2D, where chords between antibodies indicate the blocking relationships, and bins are represented by the envelopes. Consistent with the structural data, the 7 control antibodies fall into 3 non-overlapping bin clusters, since bin 2 overlaps with bin 1 and bin 3, while bin 4 and bin 5 do not overlap with any other bin.

Theoretical predictions of cross-blocking for the structural benchmark returned a complex network of epitope bins

We attempted to predict the cross-blocking pattern of the 7 controls retrospectively using 2 *in silico* metrics (see Methods). The “Fv Cα metric” models the cross-blocking of a pair of antibodies on the basis of steric hindrance between the Fv regions in their respective binding orientations, while the “common epitope AA metric” does so on the basis of overlapping antibody binding footprints as suggested by antigen residues common to the pair of epitopes. The “Fv Cα metric” heat map for the 7 controls is shown in Fig. 3A, where the red and green cells represent the structure-based predictions for blocking and sandwiching pairs of antibodies, respectively. These predictions are consistent with the experimental data (Fig. 2C), i.e., antibody pairs with one or more Cα clashes defined using a 2.5 Å cutoff radius cross-block each other experimentally, while other pairs lacking such clashes are able to sandwich one another. In contrast, the “common epitope AA metric” returned false positives (Table S2A). For example, CTL-1 (D1.3) is predicted to cross-block CTL-3 (cAbLys3) and CTL-4/4* (HyHEL-8/HyHEL-10) on account of 2 and 5

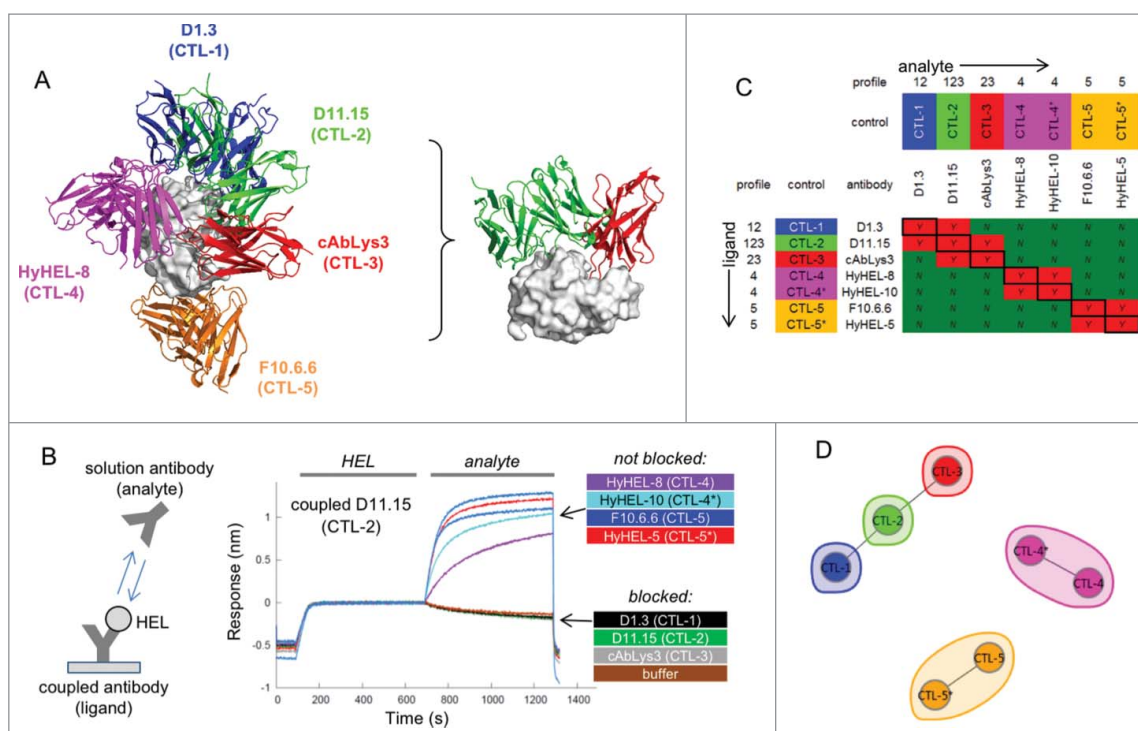


Figure 2. Epitope binning of the control antibodies and structural rationale. (A) Surface representation showing 5 control anti-HEL antibodies as ribbon diagrams superposed on the HEL surface (white space-filled model); D1.3, D11.15, cAbLys3, HyHEL-8 and F10.6.6 (CTL-1 through CTL-5, colored blue, green, red, pink, and orange, respectively). This “front view” shows dense coverage of the HEL surface by the controls. The inset highlights the close binding of CTL-2 and CTL-3 that results in their ability to cross-block one another, despite their sharing minimal overlapping epitope contacts. (B) Epitope binning analysis of 7 control antibodies (CTL-1, 2, 3, 4, 4*, 5, and 5*) using the Octet. The cartoon shows the classical sandwich assay format used, where antibody analytes were tested for their ability to bind HEL that was first captured by a coupled antibody. The overlay plot shows an example of the data obtained for coupled CTL-2; the curves are colored by analyte, as indicated. (C) A 7×7 (analyte \times ligand) heat map summarizing the epitope binning results, where green and red cells represent sandwiching and blocking pairs of antibodies, respectively. Antibodies were also assigned a “blocking profile” based upon their ability to block the primary controls (CTL-1/2/3/4/5). According to this nomenclature, profile “1” means “blocks CTL-1 and not CTL-2/3/4/5,” profile “12” means “blocks CTL-1 and CTL-2 but not CTL-3/4/5,” and so on. (D) Network blocking plot, providing an alternate way of graphing the binning results from the heat map, where chords represent the blocking relationships and the colored envelopes represent the bins.

common epitope amino acids, respectively, in contrast to the experimental “sandwiching” result for these pairs.

To assess the epitope coverage of the literature HEL antibodies as represented by the structural benchmark, we generated *theoretical* predictions on the 20 co-crystal structures (Fig. 3B) using the “Fv C α metric” validated above, experimentally, for the 7 controls. With the caveat that the predictions featuring the 13 antibodies not included in the control panel must be verified experimentally, the information from all 400 pairwise permutations of the 20 antibodies creates a complex web of 18 distinct bins, 16 of which are populated by a single antibody. These 18 epitope bins and their interconnectivities are alternatively visualized in terms of a network blocking plot (Fig. 3C), colored by “blocking profile.” Two bins are each populated by a pair of antibodies; HyHEL-8 and HyHEL-10 belong to the same bin, and 1D2L19 and D2-L29 belong to the same bin. In other words, no antibody within the panel of 20 is predicted to be able to discriminate the epitopes of 1D2L19 and D2-L29 or HyHEL-8 and HyHEL-10. In other cases, the larger interaction matrix introduces antibodies whose specificities fragment bins into sub-bins, thereby highlighting the increased epitope resolution that results from higher throughput cross-blocking analyses. For instance, 2 antibodies with near-identical epitopes (e.g., F10.6.6 and HyHEL-5) are discriminated by a single antibody (cAb-Lys2), resulting in F10.6.6 and HyHEL-5 occupying their own bins. The “structural benchmark” returns a total of 11 blocking profiles and includes examples of antibodies that simultaneously block just one control (HyHEL-8, profile 4 i.e., self-blocking), 2 controls (D2-L29;

profile 35), 3 controls (D3-L11; profile 234), 4 controls (1f9; profile 1234) or none of the 5 controls (Ab_4n1e; profile 0).

Cross-blocking data for the library clones reveals 2 main epitope communities

To characterize the epitope coverage of the library-derived panel, we performed a series of epitope binning experiments by SPR imaging using a 384-ligand array format that provided throughput higher than previously published methods.⁷ By merging 350 library clones and 7 literature controls on a single chip, we aimed to probe finer epitope resolution than may be available by considering the library clones in isolation. Each experiment tested 96 antibody analytes over a 384-ligand array, as limited by the SPR imager’s autosampler capacity, thereby necessitating 4 consecutive experiments on the same chip to address all 350 antibodies as analytes. The merged cross-blocking results from this series of experiments are summarized in the heat map shown in Fig. 4A. These data are alternately visualized as a high-level community plot (Fig. 4B), revealing 2 main communities, one populated by 176 library clones and all 7 controls (community 1, shown in purple), and another populated by 167 library clones (community 2, shown in cyan blue). These results imply that community 1 accesses epitopes on the front face of HEL (see Fig. 2A), whereas community 2 accesses epitopes on the back face of HEL (see Fig. 8B). The heavy meshing between the communities indicates that they are

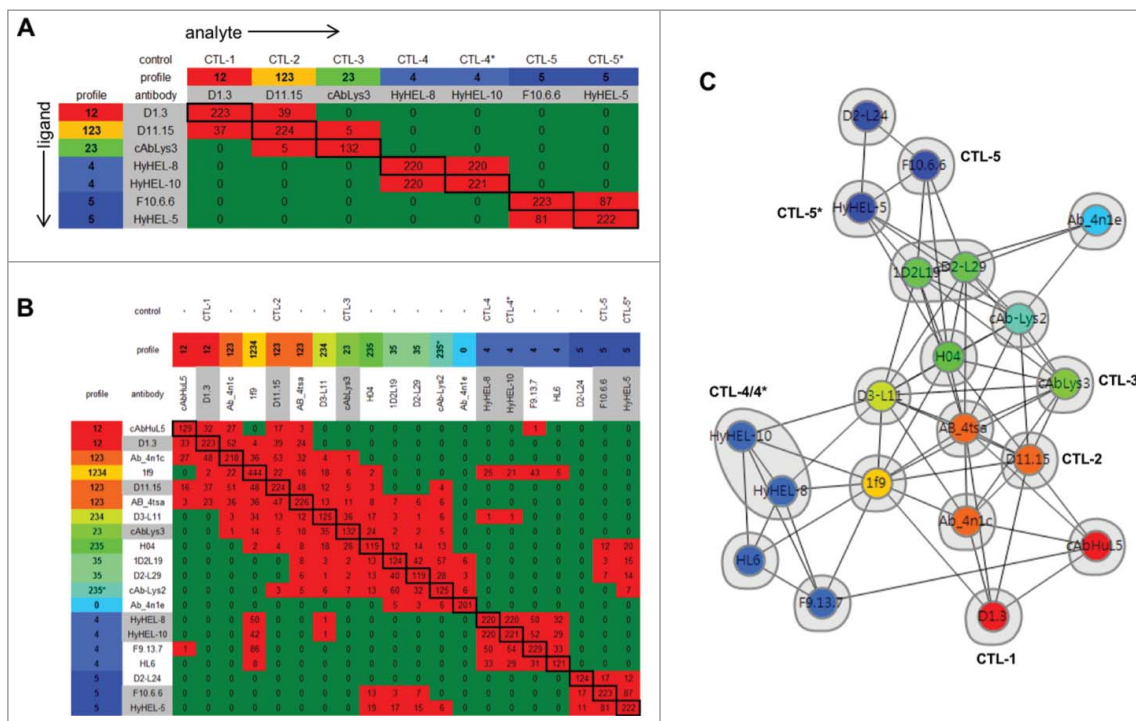


Figure 3. Assessing the collective epitope landscape of literature anti-HEL antibodies. Heat map derived from *theoretical* structure-based predictions using the Fv - C α metric for cross-blocking of (A) 7 antibodies chosen as binning controls and (B) the set of 20 literature antibodies constituting the structural benchmark (see Table 2). The values report the number of C α atoms in antibody *i* (row) within a distance of 2.5 Å of a C α atom in antibody *j* (column) after structural superposition of the HEL coordinates in the respective co-crystal structures. Note that the matrix is not symmetric. One or more C α - C α contacts so-defined leads to a theoretical “blocking” prediction for the pair of antibodies (red cells) as opposed to a non-blocking interaction (green cells). When the controls are considered as an isolated subset (in panel A), they define 5 bins. Each antibody is assigned a “blocking profile,” as described in Fig. 2’s caption. (C) Network blocking plot as an alternate graphical representation of the heat map shown in panel B, where bins are represented by envelopes (18 total), and control-based blocking profiles (11 total) are distinguished by color.

intricately interconnected by clones that cross-block both, requiring a more granular analysis to tease out finer specificities. The library therefore appears to contain epitope diversity that overlapped with and extended beyond that of the controls.

The repertoire of library epitopes is represented by a subset of clones, providing “internal” controls to facilitate future comparisons

To obtain a higher-resolution analysis of the data, we focus on a subset of 51 clones that broadly represent the library’s diversity and for which clear pairwise cross-blocking data are available in both analyte and ligand orientations. Within this smaller subset, additional details emerge (Fig. 5A). The two main communities persist, but clones such as 3F2 and 3D2 (red bin) and 4B9, 3C4, 3E10, 4C2, and 3H9 (green bin) appear to segregate from their respective bin counterparts due to their cross-blocking of non-bin clones. We further distilled the panel to a subset of 7 clones whose overlapping epitopes spanned the breadth of the library’s epitope coverage, allowing their use as internal standards against which other clones could be compared in the absence of any literature controls (Fig. 5B).

The library clones returned a larger number of “blocking profiles” relative to the structural benchmark, suggesting broader epitope coverage

Table 3 summarizes the blocking profile distribution of a set of 243 library clones for which clear assignments were

possible when the controls were injected as analyte over a 384-ligand array comprising the library and controls. Seventeen “blocking profiles” (defined in Methods) emerged in addition to an unexpected one that discriminated between the near-identical epitopes of CTL-5 and CTL-5* (blocking profile 5*). The majority of the library fell into profile 1 (91 clones) or profile 1234 (60 clones). Five other profiles (0, 5, 123, 345 and 2345) are represented by at least 10 clones, while the remaining profiles are represented by 1–3 clones each (so-called “rare” profiles). To validate the profile assignments obtained by SPR imaging, we performed an independent set of smaller, more focused experiments on the Octet. Fig. 6 shows a side-by-side technology comparison for some of the library clones that populated rare profiles in our analysis. The binning outcomes were in excellent agreement across the complementary technology platforms, confirming that the 384-ligand array SPR imaging format was reliable as a high-throughput binning platform.

The Venn diagrams shown in Fig. 7 compare the epitope coverage observed in (A) the structural benchmark and (B) the library, in terms of their blocking profiles. Our structure-based theoretical analysis of 20 antibodies from the literature returned 11 predicted profiles, all but one of which (profile 235*) are represented in the collection of 17 profiles among the library clones. Judged by the metric of the number of cross-blocking profiles, the library appears to return expanded epitope coverage relative to the structural

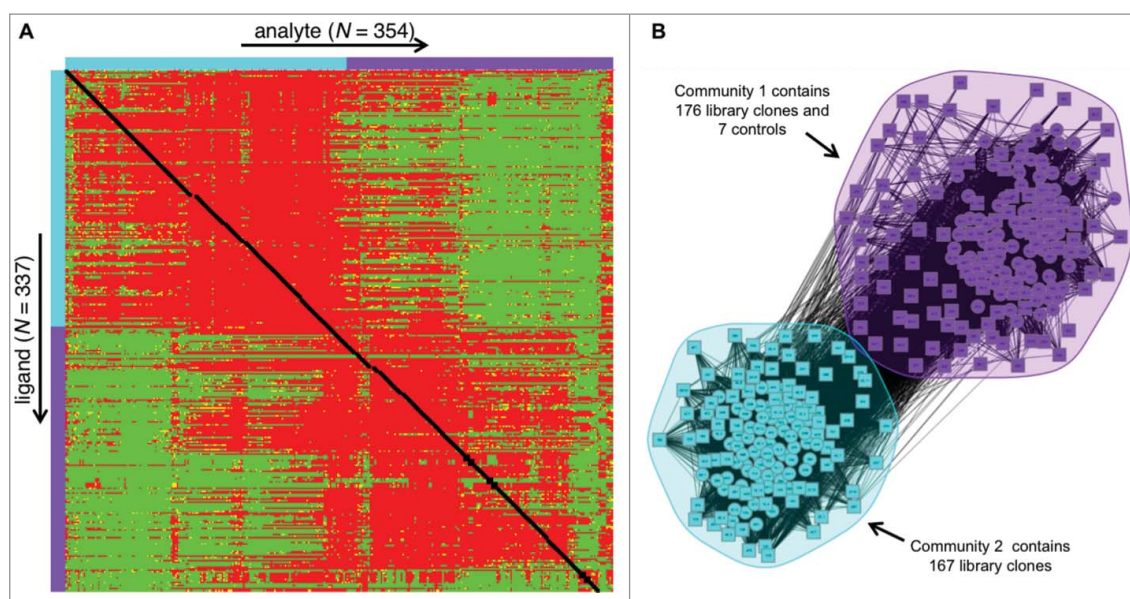


Figure 4. Merged binning analysis of a large panel of library clones and controls. (A) Heat map showing the results from a 354×337 (analyte \times ligand) matrix, totaling 119,298 pairwise interactions. The analysis included 333 library clones and all 7 controls (each in triplicate) as analytes and 319 library clones and 6 controls (each in triplicate) as ligands. Some library clones were excluded from the analysis due to their poor behavior in the assay. The solid black boxes along the diagonal indicate the self-blocking results for the majority of clones, where data was available for both analyte and ligand orientations. No self-blocking data was available for a few clones that performed poorly as ligand, such as CTL-1, which was rapidly inactivated upon acid regeneration. (B) High-level community plot of the results showing that 2 main communities emerge; community 1 (purple) is populated by 176 library clones and all 7 controls, whereas community 2 (cyan blue) is populated by 167 library clones.

benchmark, although we recognize that the library panel contains over 10 times more clones than the benchmark. Notably, antibodies that block CTL-1 exclusively (profile 1) are the most abundant ($n = 91$) in the library, but do not occur in the literature set. The next most abundant profile (1234, $n = 60$) in the library is, however, also observed in the literature set (antibody 1f9). Five other profiles, namely 13, 14, 34, 345 and 2345 with $n = 2, 2, 3, 14$ and 13 clones assigned, respectively, in the library are not represented in the literature. Based on protein-protein docking calculations, details of which are provided in the supplemental text, it appears that the 6 novel profiles are geometrically compatible with the binding footprint of an antibody on the HEL surface (Fig. S1).

Profile 0 and profile 5* demonstrate the broad epitope coverage obtained from the library. Fig. 8A shows examples of the data obtained for library clones exhibiting profile 0 (2F9, top panel) and profile 5* (1E4, bottom panel). In both cases, the assignments deduced from SPR imaging data were reinforced by Octet data. Clones belonging to profile 0 do not cross-block any of the controls. These so-called “universal sandwichers” represent 10% of the antibody panel. Antibody Ab_4n1e in the structural benchmark, which became available after we finalized the list of experimental controls, is also predicted to be a “universal sandwicher.” In contrast to the front view of HEL, which shows dense coverage by the controls (Fig. 2A), the back view shows sparse coverage, revealing a bald spot that could offer novel epitopes (Fig. 8B) relative to these controls. Indeed, the universal sandwichers mutually blocked one another, upon detailed inspection of the binning analysis shown in Fig. 4 (cyan blue community) and Fig. 5 (red bin), suggesting that they targeted a common region on the HEL

surface. While the definition of a “universal sandwicher” depends on the controls being used, in Fig S2, we visualize the binding of Ab_4n1e and CTLs 1, 3, 4 and 5, and note that the “bald spot” represents a different epitope than the one in Fig. 8B.

Clones with profile 5* display fine epitope specificity by cross-blocking F10.6.6 (CTL-5), but not HyHEL-5 (CTL-5*), despite the near-identical epitopes of these controls as compared in Fig. 8C. The set of 243 clones contained a single member (1E4) with this profile and further inspection of the full panel revealed a few more clones that belonged to profile 5*. Fig. 3 illustrates that the literature also contains a clone (cAb-Lys2) that is predicted to block HyHEL-5 (CTL-5*) and not F10.6.6 (CTL-5), but it is predicted to block other controls, D11.15 (CTL-2) and cAbLys3 (CTL-3), so it is assigned to profile 235* (see Table 2).

Inspecting the germline family distributions within the most abundant individual blocking profiles and comparing them against the baseline distribution in the set of 243 clones with assigned profiles reveals a few trends (Table S4). Profile 1234 is dominated by VH3 sequences (54/60 clones; 90%), while VH1 and VH4 sequences account for the vast majority (76/91; 83%) of profile 1 antibodies. VH4 family antibodies are 1.4-fold over-represented in profile 0 (56% versus 40%), while VK4 sequences are 2-fold over-represented (23% vs. 11%) in profile 1.

Discussion

In this work, we characterized the epitope coverage obtained using output from a naïve human *in vitro* library and HEL as a model antigen. We demonstrated that emerging SPR imaging methods employing a 384-array format

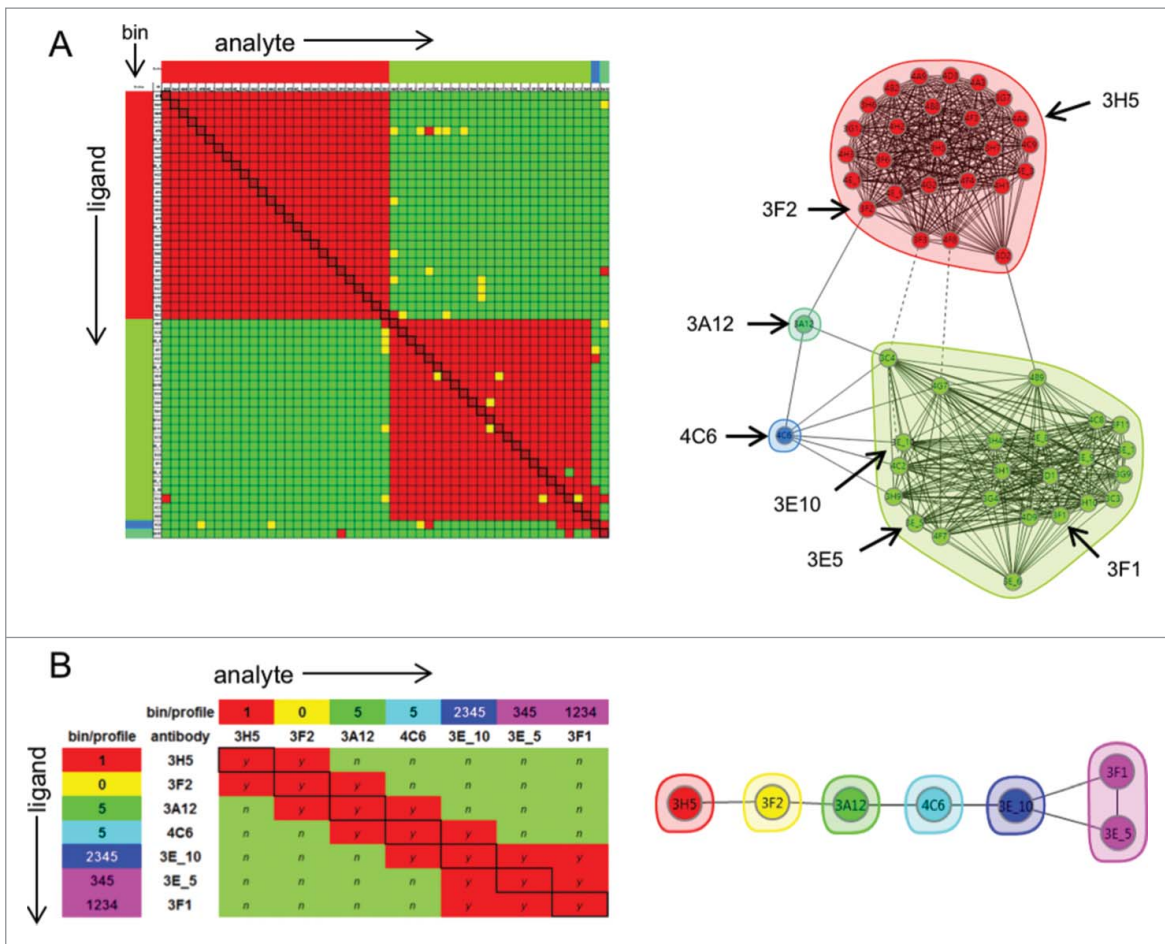


Figure 5. (A) 51×51 heat map (left) and network blocking plot (right) showing the bins deduced for a set of 51 library antibodies. In the heat map, red and green cells represent analyte/ligand pairs that blocked or sandwiched, respectively; yellow cells represent analyte/ligand pairs that gave intermediate responses that could not be assigned clearly to either category. Seven clones (indicated by the arrows) were selected as “internal controls” whose overlapping epitopes represented the breadth of the library’s epitope coverage. (B) 7×7 heat map (left) and network blocking plot (right) for the “internal controls.” Each antibody is assigned a blocking profile as described in Fig. 2’s caption.

can be used to perform epitope binning assays with superior throughput compared to those published previously,^{4,7} enabling a deeper interrogation of a library’s epitope diversity. As judged by their ability to cross-block a panel of control antibodies selected from the literature, the epitopes of the library clones appear to cover $> 75\%$ of the HEL accessible surface, with an abundance of antibodies exhibiting particular binding footprints, such as those that exclusively block CTL-1 (profile 1). In addition, the library contains clones with a diversity of binding footprints across the entire HEL solvent-accessible surface, as judged by the 17 observed blocking profiles compared to 11 for the structural benchmark. It is noteworthy that, our structural-based analysis predicted a blocking profile of 235* for the literature clone cAb-Lys2, but, upon empirically testing its ability to cross-block the controls, we found that it clearly blocked CTL-3, CTL-5 and CTL-5*, whereas its blockade of CTL-2 was unclear (data not shown). Therefore, its empirically determined profile was 35 (or perhaps, 235), and contrary to our prediction, it did not discriminate between CTL-5 and CTL-5*. We did not empirically test of all 20 literature controls, and thus our structural predictions may have over-granulized the bin count in the literature, as opposed to the empirically confirmed bin count for our library. This

example highlights that caution should be applied when predicting cross-blocking relationships based on structural data.

The germline sequence diversity of the library contributes to its broad epitope coverage since no individual light- or heavy-chain germline is observed across all 17 profiles. Antibodies with VH3 or V κ 1 sequences are found in 14 and 15 profiles, respectively, but the VH3:V κ 1 pairing itself returns only 11/17 observed profiles, and 3/6 profiles novel relative to the structural benchmark. Though no counter-selection against poly-reactivity⁹ was employed during the selections, each of the 17 observed cross-blocking profiles was populated by one or more clones with low assayed polyreactivity. Thus, the deep pool of selected binders and the high-throughput epitope binning methods limit attrition in the epitope coverage due to polyreactive clones.

The library studied in this work has produced broad epitope coverage to various therapeutic targets, which has translated into tangible benefits for some of the corresponding programs. MM-151, a clinical-stage oligoclonal cocktail of 3 antibodies targeting epidermal growth factor receptor (EGFR), is an example. The enhanced therapeutic efficacy of MM-151 has been attributed to binding of novel epitopes located on EGFR domain I and domain III that are distinct

Table 3. Thirty 2 (2⁵) theoretical blocking profiles, as defined by blockade of one or more of the 5 control antibodies (CTL-1 to CTL-5), and their experimentally-determined distribution within an *in vitro* library (total 243 antibodies). The red and green cells indicate blocked and non-blocked responses, respectively, such that blocking profile 0 means “does not block any of the controls,” blocking profile 1 means “blocks only CTL-1,” blocking profile 23 means “blocks both CTL-2 and CTL-3,” and so on. Thus, control antibodies CTL-1 through CTL-5 are defined by the blocking profiles 12, 123, 23, 4, and 5 respectively. The additional control antibodies CTL-4* and CTL-5* share the blocking profiles of their respective counterparts, CTL-4 and CTL-5. While neither the literature nor the *in vitro* library contained any clone that discriminated between CTL-4 and CTL-4*, clones that selectively blocked HyHEL-5 (CTL-5*) but not F10.6.6 (CTL-5) were found in the literature (antibody cAb-Lys2) and the *in vitro* library (antibody 1E4), represented by the additional blocking profiles 235* and 5* respectively. The blocking profiles observed within the panel of 20 literature antibodies is indicated, where “N/A” indicates an improbable profile (i.e., an antibody that can block both, CTL-1 and CTL-5), thereby reducing the number of plausible possibilities to 24. Of these, 10 were represented in the literature and an additional 7 (total 17) were represented in the *in vitro* library. See the Venn diagrams in Fig. 8 for a visual representation of the data in this table.

Blocking profile	CTL-1	CTL-2	CTL-3	CTL-4	CTL-5	CTL-5*	Predicted in literature	Observed within the <i>in vitro</i> library
0							Yes	23
1							No	91
2							No	0
3							No	0
4							Yes	3
5							Yes	9
5*							No	1
12							Yes	1
13							No	2
14							No	2
15							No (N/A)	0
23							Yes	1
24							No	0
25							No	0
34							No	3
35							Yes	2
45							No	0
123							Yes	12
124							No	0
125							No (N/A)	0
134							No	0
135							No (N/A)	0
145							No (N/A)	0
234							Yes	3
235							Yes	3
235*							Yes	0
245							No	0
345							No	14
1234							Yes	60
1235							No (N/A)	0
1245							No (N/A)	0
1345							No (N/A)	0
2345							No	13
12345							No (N/A)	0

from those of cetuximab and panitumumab.² Another example is HT-19, an anti-human epidermal growth factor receptor (HER)2 antibody being developed as an antibody-drug conjugate, which binds an epitope distinct from that of pertuzumab and trastuzumab,³ and indeed from other known domain I¹⁷ and domain III¹⁸ HER2 epitopes. A third example is the broadly neutralizing, cross-reactive antibody against α -hemolysin and 4 additional leukocidins, with superior effectiveness in combating *S. aureus* infections compared to antibodies targeting α -hemolysin alone.^{8,19} The cross-reactivity results from the specific binding to an epitope that includes a small conserved patch of amino acids, present in the background of the overall low (26%) sequence homology among the 5 targets.^{8,19}

The present study extends the scope of an earlier one carried out by Newman *et al* in 1992.¹⁴ In that study, a panel of 49 anti-HEL antibodies derived from a series of BALB/c mice immunizations were localized to different epitopes on HEL by testing their ability to cross-block a panel of control antibodies, including 3 with crystallographically-defined epitopes (D1.3, HyHEL-8, and HyHEL-5) which were also used in our control panel (CTL-1, 4 and 5*). Overall, the Newman *et al* study concluded that the epitopes of the murine antibodies collectively covered at least 80% of the lysozyme surface and speculated the availability of at least 6 non-overlapping epitopes for antibody binding. The multiple antibody:lysozyme crystal structures determined since 1992 reinforce these conclusions, as

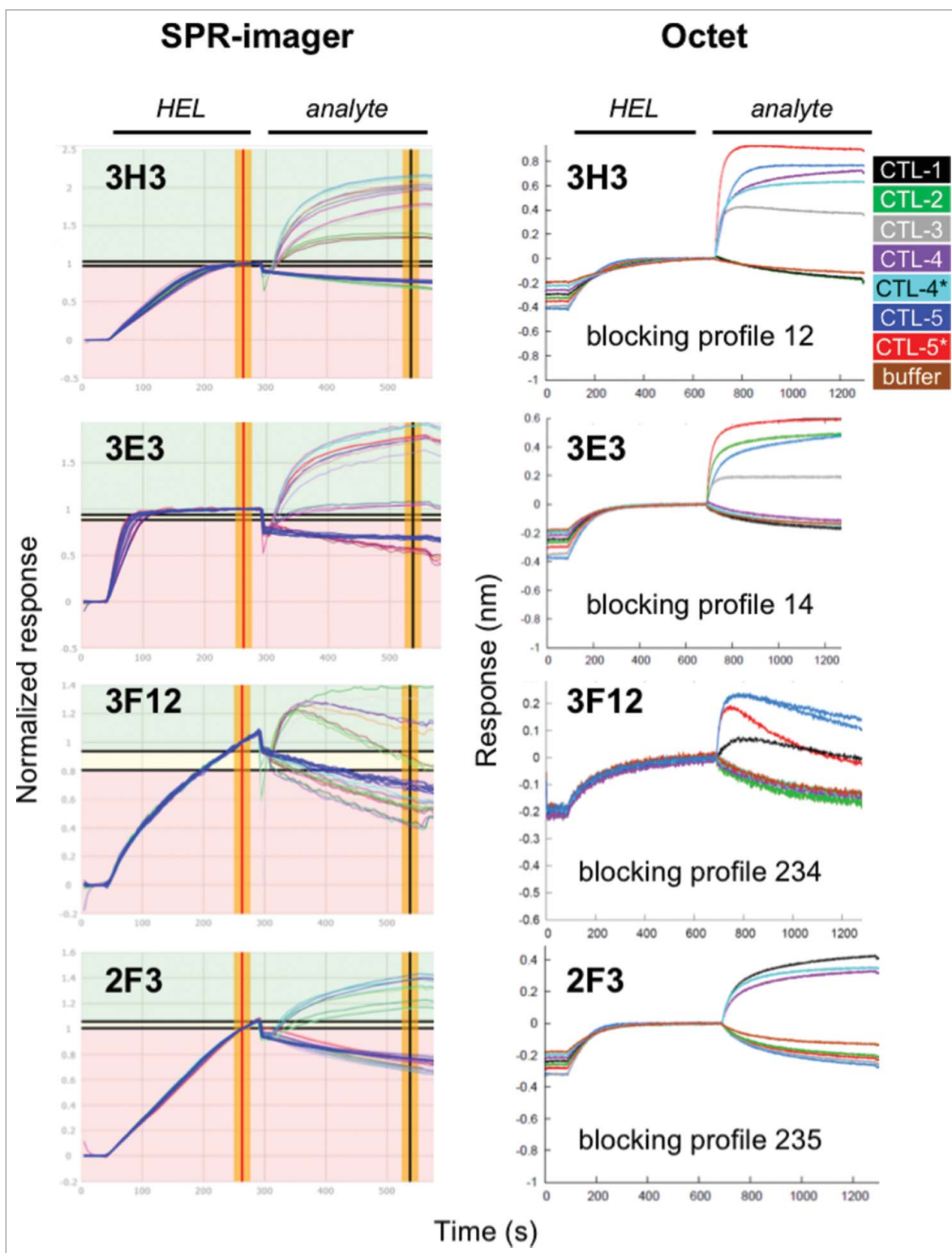


Figure 6. Merged binning analysis of a set of 243 library antibodies and 7 controls. Technology comparison of SPR imaging data (left) and Octet data (right), validating examples of rare blocking profiles. Data are grouped by the coupled antibody (named in the plot title) and the curves are either auto-colored (SPR imaging data) or colored by the antibody analyte (Octet, as indicated). The buffer analyte curves (providing the threshold for a “blocked” response) are colored blue (SPR imaging) or brown (Octet).

shown by our theoretical analysis with 20 co-crystal structures, suggesting a collective coverage of 87% of HEL’s solvent-accessible surface. Furthermore, antibodies D1.3 (CTL-1), cAbLys3 (CTL-3), HyHEL-8 (CTL-4), F10.6.6 (CTL-5) and Ab_4n1e represent 5 structurally verified non-

overlapping epitopes, leaving room for a sixth, as proposed by Newman *et al* (Fig. S2).

Our work demonstrates how high throughput epitope binning analyses can reveal deep insight into the epitope landscape of a given antibody campaign, and, by merging panels of

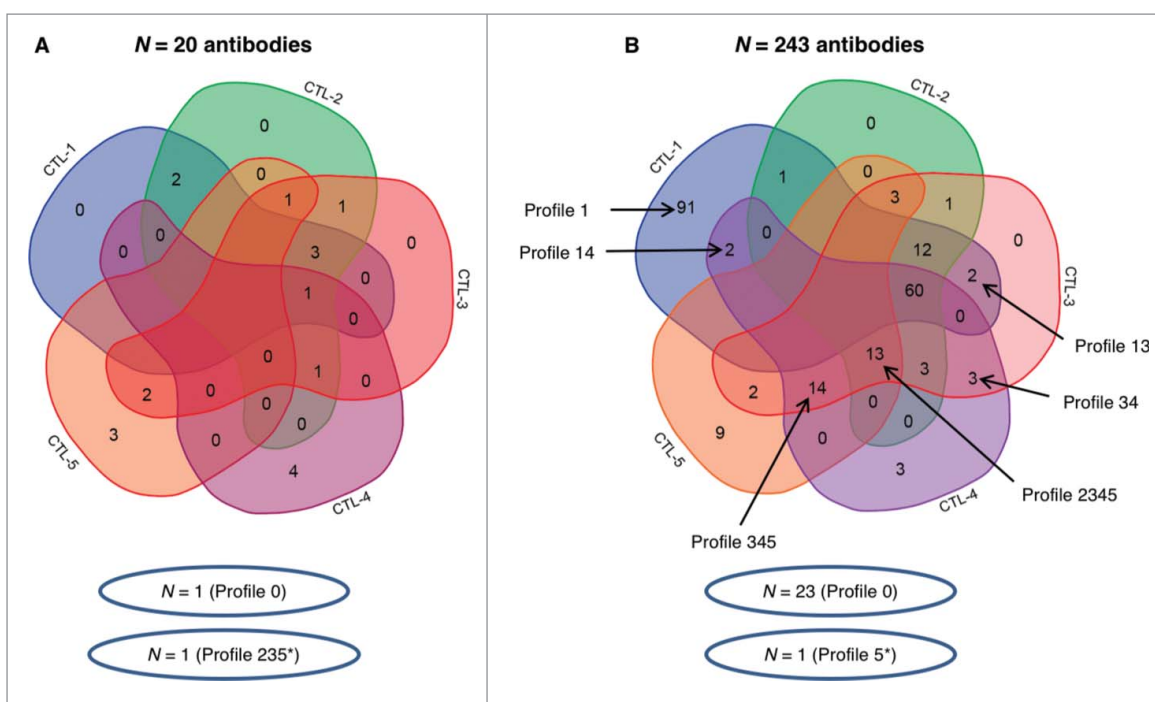


Figure 7. Venn diagrams, showing the distribution of “blocking profiles” (defined in Methods) for (A) the 20 antibodies used as our “structural benchmark” (based on structural predictions) and (B) the set of 243 library antibodies (based on empiric cross blocking data; see Table 3). The primary controls, CTLs 1–5, are schematically represented by the 5 lobes, following the coloring scheme used in Fig. 1. The number of antibodies assigned to a particular profile is provided in the overlapping regions between the relevant lobes, except for improbable profiles featuring simultaneous blockade of CTL-1 and CTL-5 (see Methods), which are left blank. Six profiles (1, 13, 14, 34, 345, and 2345) that are observed in the library-derived panel, but not predicted in the “structural benchmark,” have been highlighted. Additional profiles that are not shown include profile 235*, which is predicted in the structural benchmark, and profile 5*, which was observed in the library-derived panel. The tool provided at <http://bioinformatics.psb.ugent.be/webtools/Venn/> was used to generate the diagrams.

antibodies from different sources, how these assays can serve to benchmark libraries and selection strategies against one another. Ultimately, broad epitope coverage provides options for convergence upon the most promising lead molecules based on target biology, species cross-reactivity, developability characteristics, and intellectual property opportunities, and is thus critical to the success of therapeutic antibody programs.

Methods

Profile definitions based on cross-blocking of CTL-1 through CTL-5

Each antibody was assigned a “blocking profile” based upon its combinatorial blockade of the 5 primary controls, CTL-1 through CTL-5. Since CTL-4* and CTL-5* share the same bin as their respective counterparts CTL-4 and CTL-5 when the set of 7 controls are binned against one another (Fig. 2D), we reasoned that only 5 antibodies are required to represent the collective diversity of the 7 controls. These assignments were made using the experimental data for the library clones and the set of 7 controls, and on the basis of theoretical predictions for other antibodies in the structural benchmark (summarized in Table 3). The primary controls, along with the twin possibility of a “blocking” or “sandwich” response against a given control, give rise to $2^5 = 32$ such profiles. The profile nomenclature is based on the controls that are blocked by a given clone. For example, a clone that blocks CTL-1 and CTL-2, but not CTL-3/4/5, is assigned a “12” profile and so on. If a clone did not block any of the controls, it was assigned to profile 0.

According to this scheme, the control antibodies CTL-1, 2, 3, 4/4*, and 5/5* were defined by the blocking profiles 12, 123, 23, 4, and 5 (see heat map in Fig. 2C for their empiric cross-blocking results). Eight of the theoretical blocking profiles (15, 125, 135, 145, 1235, 1245, 1345 and 12345) were deemed improbable because they involved simultaneous cross-blockade of CTL-1 and CTL-5, whose epitopes are too far apart to be bridged by a third antibody, according to structural calculations (see Table S3). To illustrate the utility of the profile definition, consider the alternate possibilities for a clone to block CTL-1 exclusively (profile 1), or in conjunction with blocking of other controls (profiles 12, 13, 14, 123, 124, 134, 1234). Each of these profiles represents a different mode of blocking CTL-1, with partial overlap between the modes. Thus, in general, a greater number of observed profiles for a set of library clones implies better epitope coverage.

3D structure metrics for predicting antibody blocking

From a structural perspective, 2 antibodies can block one another directly, by competing for common epitope amino acid contacts, or indirectly, via steric clashes upon binding to adjacent epitopes. When co-crystal structures are available, a theoretical prediction for cross-blocking can be made by quantifying the extent of such epitope overlap or steric clashes, as described here. For each antibody:antigen complex, we computed the epitope amino acids in each co-crystal structure using a 5 Å heavy atom contact definition. Further, for each pair of co-crystal structures, we superposed the HEL coordinates and computed, 1) the number of the Fv C α atoms in one antibody

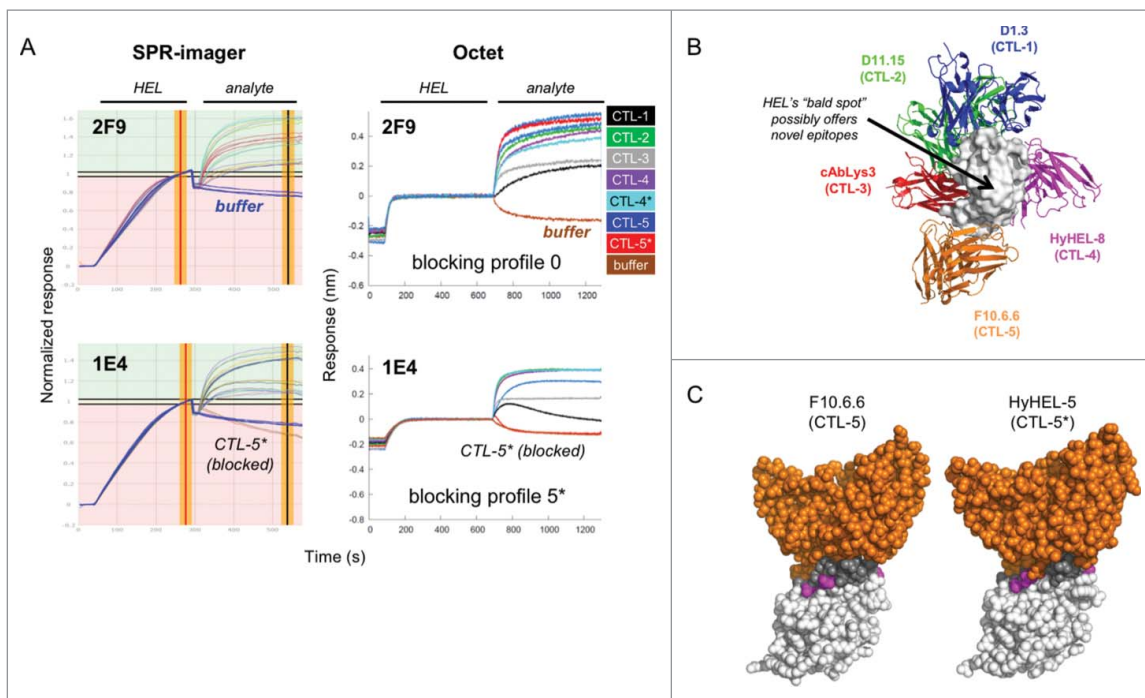


Figure 8. Structural rationale for antibody binding to HEL's "bald" spot. (A) Epitope binning data obtained by SPR imaging (left) and Octet (right) technologies confirming discovery of antibodies with profiles 0 (top) or 5* (bottom). (B) The back view of HEL reveals a "bald spot" that could offer novel epitopes, beyond those covered by the controls. (C) Model illustrating slight differences in the binding modes of F10.6.6 (CTL-5, left) and hyHEL-5 (CTL-5*, right). The structural epitope is shown in gray and purple, where gray represents HEL residues in contact with antibody (19 per antibody) and purple represents the 3 HEL residues (Ala42, Asn44 and Gly71) in contact with HyHEL-5, but not F10.6.6.

within a distance cutoff of 2.5 Å of the Fv Cα atoms in the second (Fig. 2); 2) the number of common epitope amino acids between the complexes (Table S2); and 3) the distances between the heavy-atom centroids of the respective Fv regions (Table S3). These three metrics were named the "Fv Cα metric," "common epitope AA metric" and "Fv centroid metric," respectively. Antibodies with one or more so-defined Fv Cα - Cα contacts or one or more common epitope AA are predicted to "block" each other, and otherwise "sandwich" each other. The matrix of the "Fv Cα metric" values is asymmetrical since the value for a pair of antibodies *ij* depends on the number of Fv Cα atoms in antibody *i*, but this does not affect the "block" or "sandwich" predictions using this metric.

As an example, consider antibodies D1.3 (CTL-1) and D11.15 (CTL-2), which recognize epitopes adjacent on the HEL surface. Each antibody returns 223 Cα atoms in the Fv region, of which ~40 Cα atoms share a contact (2.5 Å), indicating their close approach in binding orientations results in steric clashes (Fig. 2A); the D1.3 and D11.15 epitopes comprise 21 and 15 AA, respectively, of which 9 are common to both antibodies (Table S2A); and the Fv centroid-centroid distance is 16 Å (Table S3A). In contrast, the D1.3:F10.6.6 (or CTL-1:CTL-5) pair have zero shared Fv Cα - Cα or epitope amino acids and a centroid separation of 64 Å.

Antibody library selections against HEL

HEL-specific antibodies were isolated from a full-length human IgG1 antibody library using an in vitro yeast presentation system and associated methods as previously described.^{8,9,20} The library sequences, especially those of CDR H3, are designed to

mimic features of the human pre-immune repertoire.²⁰ Specifically, a yeast population harboring IgG diversity of $> 10^{10}$ was subjected to 3 rounds of enrichment. **Round 1:** 1×10^{10} yeast cells from each of 8 individual sub-libraries were selected against 3 mL of 100 nM biotinylated HEL (bHEL) for 10 min at 30°C, washed, and then incubated with 500 μL of streptavidin microbeads (Miltenyi Biotec) for 15 minutes at 4°C. Yeast populations of $2.9 \times 10^6 - 1.0 \times 10^7$ were rescued after capture on an LS magnetic column (Miltenyi Biotec). **Round 2:** For negative selection, 1×10^9 cells were incubated with 500 μL of streptavidin microbeads for 15 minutes at 4°C. Following incubation, the yeast-microbead suspension was applied to an LS magnetic column and the flow-through was retained. For positive selection, non-captured yeast were incubated with 750 μL of 100 nM biotinylated HEL for 10 min at 30°C, washed and incubated with 125 μL of streptavidin microbeads for 15 minutes at 4°C. Yeast populations of $9 \times 10^5 - 1 \times 10^7$ were rescued after capture on an LS magnetic column. **Round 3:** For negative selection, 5×10^8 cells were incubated with 500 μL of streptavidin microbeads for 15 minutes at 4°C. For positive selection, 1×10^8 non-captured yeast were incubated with 500 μL or 5 mL of 100 nM or 10 nM biotinylated HEL for 10 min or 30 min, respectively, at 30°C. Following incubation, cells were pelleted, washed and incubated with 1 mL of secondary labeling mix (Extravidin-R-PE, anti-human LC-FITC, and propidium iodide) on ice protected from light for 20 min and run on FACSaria II (BD Biosciences) to record 100,000 PI negative (viable) yeast events. The data were used to sort 5,000–20,000 yeast cells with PtdIns negative, LC-FITC positive (IgG presenting), and EA-R-PE positive (bHEL-binding) phenotypes. A total of 2940 unique clones were produced and

characterized for HEL binding by Octet,¹⁰ leading to a final selection of 350 antibodies included in this binning study.

Binding kinetics and affinities

The binding kinetics of soluble HEL (Sigma product number L6876) toward immobilized anti-HEL antibodies, were determined at 25°C and in a running buffer of phosphate-buffered saline (PBS) pH 7.4 + 0.01% Tween20 using a ProteOn-XPR36 surface plasmon resonance (SPR) biosensor (BioRad Inc.). A capture-based one-shot kinetic method was used, as described by Nahshol *et al.*²¹ Goat F(AB')₂ anti-human IgG Fc (Cappel product number 55053, lot number 04459) served as the capture reagent and was coated onto the ligand channels of a GLC chip by standard amine-coupling or was biotinylated (using Pierce EZ-link LC-LC linker) and captured via an NLC (neutravidin) chip; final levels of the capture reagent were ~3,000 RU (GLC) or 2,000 RU (NLC). Anti-HEL antibodies (all formatted as human, aglycosylated, IgG1-Fc) were captured at 5 µg/ml along the ligand channels to low levels (100 - 300 RU) and then HEL was injected along the analyte channels at concentrations of 70, 14, 2.8, 0.56, 0.11, and 0 nM (or, in some experiments, 100, 20, 4, 0.8, 0.16, and 0 nM). Association and dissociation times of 3 min and 15 min were allowed. The capture surfaces were regenerated with 75 mM phosphoric acid after each capture cycle. The reaction spot data were “double-referenced” by subtracting the interspot (reference) data and the buffer analyte data,²² and the resulting sensorgrams were fit globally to a simple Langmuir model using the ProteOn Manager software.

Epitope binning experiments

An SPR imager was used (IBIS MX96) for the epitope binning experiments as described previously,⁷ but with a modified continuous flow microspotter (CFM) and immobilization routine designed to increase the number of reaction surfaces addressed to 384. A printhead device with different geometry flow cells (130 µm × 435 µm) than previously employed (400 µm × 500 µm) was used to amine-couple the entire set of 380 antibodies (comprising 350 antibodies from the library and 7 controls in triplicate) on a single Xantec 200 M prism (Xantec GmbH, Germany). The unattended print routine immobilized the 380 antibodies in 8 consecutive prints by cycling activating reagent for 5 mins, the antibodies for 7 mins, and finally rinsing with running buffer (PBS + 0.01% Tween-20). The chip printed with a 384-antibody array was then docked into the SPR imager (IBIS MX96) for online quenching with 1.0 M ethanolamine.HCl pH 8.5. Epitope binning experiments were performed using a classical sandwich assay format, where a binding cycle involved capturing 100 nM HEL for 240 s, immediately injecting one of the competing antibody analytes at 20 µg/ml for 240 s, allowing a 30 s dissociation phase, and finally injecting a single 20 s regeneration pulse of 75 mM phosphoric acid. A plate of 96 antibody analytes was addressed per unattended run, as limited by the auto-sampler's capacity. Buffer analytes were drawn from containers or vials and interspersed throughout the assay after

every 12 antibody analytes to provide the blanks used in the data analysis. The entire panel of 380 antibody analytes was addressed in 4 consecutive experiments on the same chip taking 6 d and consuming a total of 60 µg HEL and 3 µg antibody for each analyte.

The resultant 153,664 binding sensorgrams from the 4 experiments were then merged in the binning module of ECTO (Wasatch Microfluidics, US), a software tool for processing and analyzing epitope binning data. ECTO includes a series of advanced data analysis routines that were used to help identify non-ideal or problematic behaviors from analytes and ligands. This toolkit was especially useful when curating the 144,400 analyte/ligand pairs, representing the 380 × 380 (analyte × ligand) interaction matrix, that made up the final merged data set (presented in Fig. 4). For example, ~10% of the antibodies behaved poorly as ligands, either due to their inefficient coupling under the conditions used or their inactivation upon acid regeneration, but were highly active in solution. The software was able to correctly identify unusable ligand data based on its signal level and blocking result frequency while preserving the solution binding information from those same species for further analysis. By applying user-defined threshold settings, analyte/ligand pairs are classified as blocked or not blocked (sandwiching) and results are graphed in various ways. For example, to construct a heat map, ligands are represented in rows, analytes are represented in columns, and cells are colored according to whether a given analyte/ligand pair showed a blocked response (red) or a sandwiching response (green). An analyte/ligand pair that gives an intermediate response falling between these threshold settings is shown by a yellow cell. The heat map is sorted by advanced clustering routines and the self-blocking interactions (representing the use of the same antibody in the role of analyte and ligand) are shown along the diagonal with thick box borders in black. The results from a heat map are alternately graphed in terms of a network blocking plot, where antibodies are represented as nodes and connected to other antibodies by chords to represent the blocking relationships. A dotted chord indicates a blocking relationship observed in only one orientation. Antibodies displaying similar blocking relationships are inscribed by an envelope to show that they belong to the same “bin.” A community plot is a low-resolution version of a network blocking plot using less stringent threshold settings for comparison criteria.

Confirmatory binning experiments were performed on smaller panels in lower throughput assays using BLI technology (Octet-Red384 equipped with amine-reactive sensors, Pall-Fortebio). Similar conditions were used as described above, except that antibodies were coupled at 30 µg/ml in a coupling buffer of 100 mM 2-(N-morpholino)ethanesulfonic acid (pH 4.0) and the running buffer for the binning was PBS + 0.05% Tween-20 + 5 g/l bovine serum albumin. Octet data were processed and displayed as overlay plots using in-house scripts.

Disclosure of potential conflicts of interest

No potential conflicts of interest were disclosed.

Acknowledgements

We thank Kevin Lindquist, from Rinat-Pfizer, for developing biosensor data analysis tools used to generate the Octet data overlay plots and the isoaffinity plot. We also thank Urszula Sharples, Beth Sharkey and Sarat Pudi for generating reagents used in the study, and Tushar Jain for assistance with the Fv modeling.

ORCID

Patricia Estep  <http://orcid.org/0000-0003-3055-4074>
Rebecca Hurley Niles  <http://orcid.org/0000-0001-8568-3047>

References

- Reichert JM. Antibodies to watch in 2016. *MAbs* 2016; 8:197-204; PMID:26651519; <http://dx.doi.org/10.1080/19420862.2015.1125583>
- Arena S, Siravegna G, Mussolin B, Kearns JD, Wolf BB, Misale S, Lazzari L, Bertotti A, Trusolino L, Adjei AA, et al. MM-151 overcomes acquired resistance to cetuximab and panitumumab in colorectal cancers harboring EGFR extracellular domain mutations. *Sci Transl Med* 2016; 8:324ra14; PMID:26843189; <http://dx.doi.org/10.1126/scitranslmed.aad5640>
- Pauthner M, Yeung J, Ullman C, Bakker J, Wurch T, Reichert JM, Lund-Johansen F, Bradbury AR, Carter PJ, Melis JP. Antibody engineering & therapeutics, the annual meeting of the antibody society December 7–10, 2015, San Diego, CA, USA. *MAbs* 2016; 8:617-52; PMID:26909869; <http://dx.doi.org/10.1080/19420862.2016.1153211>
- Abdiche YN, Harriman R, Deng X, Yeung YA, Miles A, Morishige W, Boustany L, Zhu L, Izquierdo SM, Harriman W. Assessing kinetic and epitopic diversity across orthogonal monoclonal antibody generation platforms. *MAbs* 2016; 8:264-77; PMID:26652308; <http://dx.doi.org/10.1080/19420862.2015.1118596>
- Chan CE, Lim AP, MacAry PA, Hanson BJ. The role of phage display in therapeutic antibody discovery. *Int Immunol* 2014; 26:649-57; PMID:25135889; <http://dx.doi.org/10.1093/intimm/dxu082>
- Fuh G. Synthetic antibodies as therapeutics. *Expert Opin Biol Ther* 2007; 7:73-87; PMID:17150020; <http://dx.doi.org/10.1517/14712598.7.1.73>
- Abdiche YN, Miles A, Eckman J, Foletti D, Van Blarcom TJ, Yeung YA, Pons J, Rajpal A. High-throughput epitope binning assays on label-free array-based biosensors can yield exquisite epitope discrimination that facilitates the selection of monoclonal antibodies with functional activity. *PLoS One* 2014; 9:e92451; PMID:24651868; <http://dx.doi.org/10.1371/journal.pone.0092451>
- Rouha H, Badarau A, Visram ZC, Battles MB, Prinz B, Magyarics Z, Nagy G, Mirkina I, Stulik L, Zerbs M, et al. Five birds, one stone: neutralization of alpha-hemolysin and 4 bi-component leukocidins of *Staphylococcus aureus* with a single human monoclonal antibody. *MAbs* 2015; 7:243-54; PMID:25523282; <http://dx.doi.org/10.4161/19420862.2014.985132>
- Xu Y, Roach W, Sun T, Jain T, Prinz B, Yu TY, Torrey J, Thomas J, Bobrowicz P, Vasquez M, et al. Addressing polyspecificity of antibodies selected from an in vitro yeast presentation system: a FACS-based, high-throughput selection and analytical tool. *Protein Eng Des Sel* 2013; 26:663-70; PMID:24046438; <http://dx.doi.org/10.1093/protein/gzt047>
- Yu Y, Mitchell S, Lynaugh H, Brown M, Nobrega RP, Zhi X, Sun T, Caffry I, Cao Y, Yang R, et al. Understanding ForteBio's Sensors for High-Throughput Kinetic and Epitope Screening for Purified Antibodies and Yeast Culture Supernatant. *J Biomol Screen* 2016; 21:88-95; PMID:26442912; <http://dx.doi.org/10.1177/1087057115609564>
- Lefranc MP, Pommie C, Ruiz M, Giudicelli V, Foulquier E, Truong L, Thouvenin-Contet V, Lefranc G. IMGT unique numbering for immunoglobulin and T cell receptor variable domains and Ig superfamily V-like domains. *Dev Comp Immunol* 2003; 27:55-77; PMID:12477501; [http://dx.doi.org/10.1016/S0145-305X\(02\)00039-3](http://dx.doi.org/10.1016/S0145-305X(02)00039-3)
- Kelly RL, Sun T, Jain T, Caffry I, Yu Y, Cao Y, Lynaugh H, Brown M, Vasquez M, Wittrup KD, et al. High throughput cross-interaction measures for human IgG1 antibodies correlate with clearance rates in mice. *MAbs* 2015; 7:770-7; PMID:26047159; <http://dx.doi.org/10.1080/19420862.2015.1043503>
- Berman HM, Westbrook J, Feng Z, Gilliland G, Bhat TN, Weissig H, Shindyalov IN, Bourne PE. The Protein Data Bank. *Nucleic Acids Res* 2000; 28:235-42; PMID:10592235; <http://dx.doi.org/10.1093/nar/28.1.235>
- Newman MA, Mainhart CR, Mallett CP, Lavoie TB, Smith-Gill SJ. Patterns of antibody specificity during the BALB/c immune response to hen eggwhite lysozyme. *J Immunol* 1992; 149:3260-72; PMID:1431104
- Decanniere K, Transue TR, Desmyter A, Maes D, Muyldermans S, Wyns L. Degenerate interfaces in antigen-antibody complexes. *J Mol Biol* 2001; 313:473-8; PMID:11676532; <http://dx.doi.org/10.1006/jmbi.2001.5075>
- De Genst E, Silence K, Decanniere K, Conrath K, Loris R, Kinne J, Muyldermans S, Wyns L. Molecular basis for the preferential cleft recognition by dromedary heavy-chain antibodies. *Proc Natl Acad Sci U S A* 2006; 103:4586-91; PMID:16537393; <http://dx.doi.org/10.1073/pnas.0505379103>
- Zhou H, Zha Z, Liu Y, Zhang H, Zhu J, Hu S, Shen G, Cheng L, Niu L, Greene MI, et al. Structural insights into the down-regulation of over-expressed p185(her2/neu) protein of transformed cells by the antibody chA21. *J Biol Chem* 2011; 286:31676-83; PMID:21680730; <http://dx.doi.org/10.1074/jbc.M111.235184>
- Fisher RD, Ultsch M, Lingel A, Schaefer G, Shao L, Birtalan S, Sidhu SS, Eigenbrot C. Structure of the complex between HER2 and an antibody paratope formed by side chains from tryptophan and serine. *J Mol Biol* 2010; 402:217-29; PMID:20654626; <http://dx.doi.org/10.1016/j.jmb.2010.07.027>
- Badarau A, Rouha H, Malafa S, Battles MB, Walker L, Nielson N, Dolezilskova I, Teubenbacher A, Banerjee S, Maierhofer B, et al. Context matters: The importance of dimerization-induced conformation of the LukGH leukocidin of *Staphylococcus aureus* for the generation of neutralizing antibodies. *MAbs* 2016; 8:1347-1360; PMID:27467113
- Vasquez M, Feldhaus M, Gerngross TU, Wittrup KD, inventors; Adimab Inc, assignee. Rationally designed, synthetic antibody libraries and uses therefor. WO2009036379. 2009
- Nahshol O, Bronner V, Notcovich A, Rubrecht L, Laune D, Bravman T. Parallel kinetic analysis and affinity determination of hundreds of monoclonal antibodies using the ProteOn XPR36. *Anal Biochem* 2008; 383:52-60; PMID:18782554; <http://dx.doi.org/10.1016/j.ab.2008.08.017>
- Myszka DG. Improving biosensor analysis. *J Mol Recognit* 1999; 12:279-84; PMID:10556875; [http://dx.doi.org/10.1002/\(SICI\)1099-1352\(199909/10\)12:5%3c279::AID-JMR473%3e3.0.CO;2-3](http://dx.doi.org/10.1002/(SICI)1099-1352(199909/10)12:5%3c279::AID-JMR473%3e3.0.CO;2-3)